

BARS AND DARK MATTER HALO CORES

J. A. SELLWOOD

Rutgers University, Department of Physics & Astronomy,
136 Frelinghuysen Road, Piscataway, NJ 08854-8019
sellwood@physics.rutgers.eduSubmitted to *ApJ*

ABSTRACT

Self-consistent bars that form in galaxies embedded within cuspy halos are unable to flatten the cusp. Short bars form in models with quasi-flat rotation curves. They lose angular momentum to the halo through dynamical friction, but the continuous concentration of mass within the disk as the bar grows actually compresses the halo further, overwhelming any density reduction due to the modest angular momentum transfer to the halo. Thus the Weinberg-Katz proposed solution to the non-existence of the predicted cuspy halos from CDM simulations would seem to be unworkable. I also find that the concerns over the performance of N -body codes raised by these authors do not apply to the methods used here.

Subject headings: galaxies: formation — galaxies: kinematics dynamics

1. INTRODUCTION

It now seems that the cuspy density profile of halos which form in simulations of the dark matter (DM) component is a robust and reproducible feature of the collisionless dynamics of halo formation (*e.g.* Power *et al.* 2002). The precise slope of the inner profile, if it can indeed be characterized by a power law, is still disputed, but all agree that the DM density rises steeply towards the center.

Tests of this prediction require estimates of the DM density profiles in galaxies. In principle, the mass profile of DM can be deduced from rotation curve measurements, once the contribution due to the observed baryonic material has been subtracted. Attention has generally focused on DM dominated galaxies, such as low surface brightness (LSB) or dwarf galaxies, because of their believed smaller relative baryonic content today.

There is a substantial and increasing body of high-resolution optical data to indicate that small and LSB galaxies have slowly rising rotation curves (*e.g.* Rubin *et al.* 1985; Courteau 1997; Palunas & Williams 2000; Blais-Ouellette *et al.* 2001; de Blok *et al.* 2001; Matthews & Gallagher 2002) indicating that their DM halos today have rather uniform density cores irrespective of the stellar contribution.

Estimates of the DM density profile in larger galaxies are more difficult because of the relatively greater baryonic contribution to the rotation curve. Weiner *et al.* (2001) have made the only *dynamical* estimate of the baryonic mass of a galaxy in the literature, finding that baryons dominate the inner galaxy and the DM halo has very low central density. A similar result is argued, though slightly less directly, for the Milky Way (Binney & Evans 2001).

A much less direct, but more general, argument was advanced by Debattista & Sellwood (1998, 2000). The fact that bars appear not to have been slowed by friction places an upper bound to the central DM density in barred galaxies. The dimensionless parameter $\mathcal{R} = D_L/a_B$, with D_L is the radius of corotation and a_B the semi-major axis of the bar, is measured to lie in the range $1 \lesssim \mathcal{R} \lesssim 1.4$ in several cases (Aguerri *et al.* 2002), while other, less direct, evidence also suggests that bars end only slightly inside their corotation circles. Debattista & Sellwood found that

such low values of \mathcal{R} can be sustained only if the halo has a low central density.

Low central densities of DM in galaxies today need not be a problem for the currently favored Λ CDM model if the cusps could be subsequently erased during galaxy formation or evolution. At least three ideas to lower the central DM density have been proposed:

- Binney, Gerhard & Silk (2001), and others have proposed that the halo profile is altered by adiabatic compression as the gas cools followed by impulsive outflow of a large fraction of the baryon mass. One possible mechanism to produce such an outflow might be a burst of star formation. The idea was examined by Navarro, Eke & Frenk (1996) and by Gnedin & Zhao (2002), who found that only a mild reduction in the central DM density could be achieved in this way. Gnedin & Zhao tested the extreme case that 100% of the baryonic component was somehow blasted out instantaneously, yet found that even in this deliberately unrealistic case, the central density decreased by little more than a factor 2, unless the initial baryons were unrealistically concentrated to the halo center.
- Milosavljević *et al.* (2002) point out that a binary supermassive black hole (BH) pair created from the merger of two galaxy fragments will eject DM (and stars) from the center of the merger remnant. They also suggest that the DM mass removed for a given final BH mass is greater if the final BH is built up in a series of mergers each having correspondingly lower mass BHs. While this mechanism must operate wherever binary BHs have been formed, the radial extent over which the mass is reduced is rather limited (typically a few hundred pc), whereas the radial extent of DM cores in brighter galaxies (*e.g.* Weiner *et al.* 2001) is too large to be accounted for by this mechanism alone. Furthermore, cores are observed in DM-dominated galaxies with insignificant bulges which, are likely to have very low-mass BHs (Gebhardt *et al.* 2001; Ferrarese & Merritt 2001), if they contain BHs at all.

- El-Zant *et al.* (2001) propose that the cusp in the halo density can be erased by dynamical friction between orbiting mass clumps. Weinberg & Katz (2001) draw attention to the earlier paper by Hernquist & Weinberg (1992) which showed that a rotating, imposed bar in the disk could also flatten the cusp through dynamical friction.

This paper explores and clarifies the possible role played by bars. I find that the mechanism proposed by Weinberg & Katz (2001) is, in fact, overwhelmed by on-going compression leading to a gradual *increase* in halo density. The possible role of satellites will be explored in a later paper.

Concerns about the simulations and conclusions of Debattista & Sellwood (1998, 2000) have been expressed recently. This paper also addresses the numerical issues raised by Weinberg & Katz (2001). The criticisms of Valenzuela & Klypin (2002) will be addressed in a future paper.

2. MECHANISMS AND NUMERICAL ISSUES

Dynamical friction in a perfectly collisionless system (Chandrasekhar 1943) is caused by the density wake induced by a massive perturber moving through a background of low-mass particles; the gravitational attraction between the wake and the perturber is the retarding force. The standard analysis (Binney & Tremaine 1987) neglects the interactions between the background particles themselves, which would tend to increase the concentration of the wake, and applies to a steady state in which the introduction of the perturber is ignored. The wake would not form instantly if a perturber were suddenly introduced, but would build up over the time scale on which the orbits are deflected.

The analysis becomes more complicated for a bar rotating in a galaxy because orbits are periodic. Repeated encounters with a rotating bar lead to secular changes only at resonances (Tremaine & Weinberg 1984), but friction is still expected (Weinberg 1985) because resonant particles generally gain angular momentum from the bar. A bi-symmetric density excess develops in a non- or slowly-rotating halo as orbits become trapped or linger “behind” the moving bar giving rise to the frictional force which slows the bar.

Hernquist & Weinberg (1992, hereafter HW92) and Weinberg & Katz (2001, hereafter WK01) describe experiments in which the angular momentum transferred to the halo through dynamical friction from a driven, imposed bar lowers the density of the inner halo substantially. In the later paper, they suggest that simulations of very high quality are needed in order to reproduce the proper dynamical friction when the DM has a cusped density profile.

There is no doubt that simple systems with pseudo-harmonic cores are much easier to simulate than those with steep density gradients; the large ranges of densities and time-scales present in cusped halos obviously demand increased numerical care. But WK01 suggest the difficulties are yet greater because there are important resonances between the bar and particles within the cusp where a small fraction of the mass resides. They argue that particle noise can destroy resonances if an orbit is scattered frequently and suggest that this delicate effect would inhibit the correct evolution in low-quality simulations.

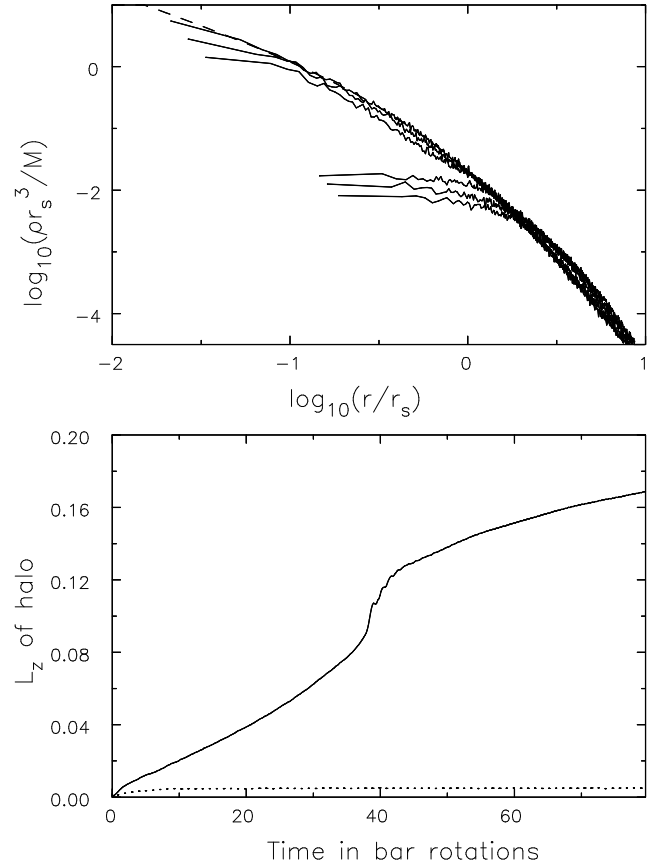


FIG. 1.— Top: The density profile at different times in a model to confirm the result from HW92. The curves are drawn at intervals of 16 bar rotations, with the later times having lower central densities. The dashed curve shows the theoretical density profile of the Hernquist model. Bottom: The angular momentum of the halo as a function of time in the same simulation. The total change of angular momentum is 32 times that contained in the bar. The dotted curve is described in §3.4.

The purpose of the experiments described in §3 is to determine the numerical parameters required to reveal the correct behavior. I find that cusps can be flattened in simulations with relatively modest numbers of particles and the rate of evolution does depend on N , in the sense that evolution with too few particles can be faster than the correct rate. This result, while consistent with that found by WK01 in their simulations using the SCF method (Hernquist & Ostriker 1992), disagrees with their prediction for collision-dominated methods; it is possible that a different N -dependence might be found in other types of N -body code.

3. DRIVEN BARS

HW92 and WK01 report artificial experiments with bars driven at constant angular rates. In one case, HW92 employed a Hernquist (1990) halo model, which has the density profile

$$\rho(r) = \frac{Mr_s}{2\pi r(r_s + r)^3}, \quad (1)$$

having an inner r^{-1} density cusp and an outer slope that is steeper than NFW. Here, M is the total mass of the halo and r_s is the break radius of the profile. They introduced a rotating quadrupole field of the form

$$\Phi_{\text{bar}} = -\frac{GM_{\text{bar}}}{a} \frac{\alpha R_*^2}{(\beta^2 + R_*^2)^{5/2}} \sin^2 \theta e^{2i(\phi - \Omega_p t)}, \quad (2)$$

where $R_* = R/a$, R is the cylindrical radius, (r, θ, ϕ) are the usual spherical polar coordinates, and M_{bar} and Ω_p are the mass and pattern speed of the bar. This expression, which behaves properly as a quadrupole for both small and large r , was derived from a fit to the analytical field of an inhomogeneous ($n = 2$) Ferrers bar with axes $a : b : c = 1 : 0.5 : 0.1$ for which the best fit dimensionless parameters are: $\alpha \simeq 0.1404$ and $\beta \simeq 0.4372$. Note that they employed only this $m = 2$ quadrupole term of the bar field and ignored all other terms, including the monopole term which they omitted in order to avoid adding mass in the center of the equilibrium halo.

HW92 chose the semi-major axis of the bar, a , equal to the break radius, r_s , of the Hernquist profile, the bar mass to be 30% of the halo mass interior to this radius (*i.e.* 7.5% of the total halo mass) and drove the bar at a constant pattern speed which placed corotation also at r_s . They found that the density within the cusp decreased gradually at first, but after about 50 bar rotations a rather sudden density decrease completely erased the cusp.

Figure 1 shows the result from an experiment as similar as I was able to construct to that reported by HW92. In this case, I used the PM+SH method described in Appendix A; the spherical grid had 200 radial shells, included only the $l = 0 \& 2$ terms in the self-gravity of the halo, and employed just 100 000 particles. Tests with different time steps, numbers of grid shells and larger numbers of particles confirm that the results shown are insensitive to these parameters. The evolution of the density profile in the top panel closely resembles that shown in their Figure 10, while the change of angular momentum of the halo, shown in the lower panel, should be compared to their Figure 4. The agreement with their old results is completely satisfactory.

Even though the set-up is artificial, and the angular momentum given to the halo exceeds that contained in the imposed bar by much more than an order of magnitude, the experiment illustrates that the halo density profile can, in principle, be changed substantially by dynamical friction.

3.1. Parameter tests

Figure 2 shows the radius containing 1% of the halo mass, which obviously increases as the central density drops, as function of time from this and other experiments using the same halo, bar model and (mostly) numerical code. Figure 2(a) shows results from four simulations in which the bar length, a , and its mass were varied, but the axis ratio, pattern speed and all numerical parameters were held fixed. The bar mass was always 30% of the halo mass interior to $r = a$. The run with $x = a/r_s = 1$ is that shown in Figure 1. The behavior when the bar length is reduced is qualitatively similar, but the dramatic change occurs later as the driving quadrupole field is made

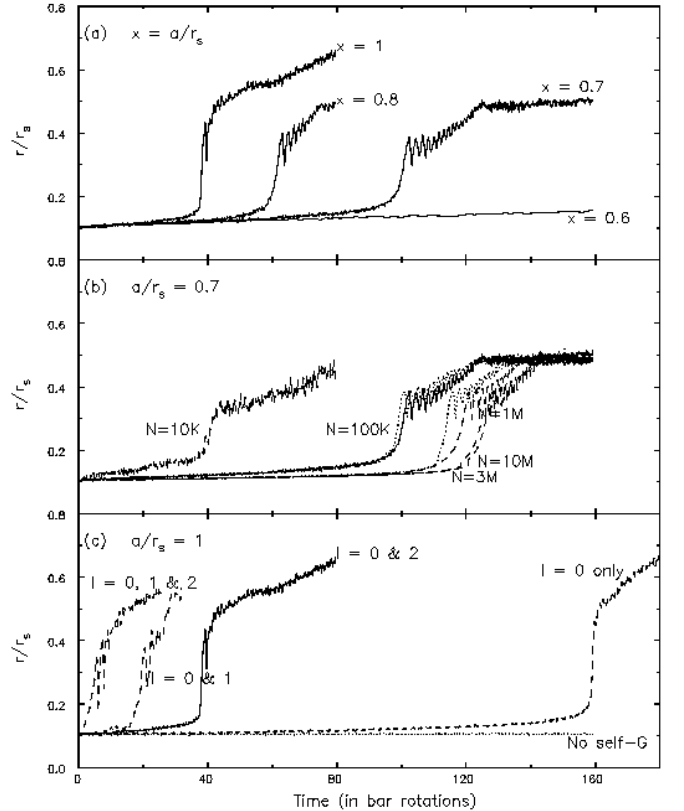


FIG. 2.— Results from many different simulations with a driven, imposed bar inside a cuspy Hernquist halo. (a) The effect of changing the bar half-length, a , relative to r_s , the break radius of the halo. (b) The effect of changing particle number. The solid curve for $N = 100K$ is reproduced from (a), the dashed curves are for the same physical parameters but different numbers of particles. The two dotted curves are from runs with the SCF code ($N = 100K$ & $N = 1M$) instead of the PM+SH code employed for all others. (c) The effect of changing the order of expansion for the gravitational field. The solid curve is for $x = 1$ reproduced from (a) and the dashed lines indicate other runs with different numbers of terms in the force calculation. The dotted line shows the effect of ignoring the self-gravity of the halo particles.

weaker, and did not occur, at least for 160 bar rotations, when $x = 0.6$.

Figure 2(b) shows the effect of changing the particle number. The solid curve is reproduced from the $x = 0.7$ case in (a), and the various dashed curves show the results obtained as the particle number is varied while all physical, and other numerical, parameters are held fixed. The trend in this diagram is clearly that the density decrease is delayed as the numerical quality (particle number) is improved. Moreover, the dotted curves show the results for two cases in which the field is calculated using the SCF method (Hernquist & Ostriker 1992) while starting from the same initial particle distribution; the differences between the results from the PM+SH and SCF codes are relatively minor.

The data for $x = 0.7$ in Figure 2(b) hint that the time scale is converging as $N \rightarrow 10M$. This slow convergence for the weaker bar case contrasts with the behavior in the strong bar case (not shown); tests with different particle numbers when $a = r_s$ ($x = 1$) reveal that the rate of evolution is identical when $N \gtrsim 100K$, although it is yet

more rapid for $N = 10K$ – *i.e.* convergence when $x = 1$ occurs for a particle number some 100 times smaller than for the weaker bar case.

Aside from the changing time-scale, the curves in Figure 2(b) are remarkably consistent over three orders of magnitude in particle number. The difference in time-scale clearly has little effect on the outcome and the eventual density decrease is almost independent of N .

Figure 2(c) shows the consequences of changing the number of terms employed to determine the field of the halo particles, all for the longest and most massive bar in these tests which has $a = r_s$. The solid line reproduces the $x = 1$ result from (a) while the dashed curves are for the same particle distribution and bar, but employing the indicated expansion terms. These results show that the evolution is accelerated by including $l = 1$ terms, and generally that fewer terms in the force determination delay the density decrease, which always occurs. Adding $l = 3$ and/or $l = 4$ terms has little effect; the rate of evolution seems to be determined largely by which of the $0 \leq l \leq 2$ terms are active.

The horizontal dotted line in Figure 2(c) shows the consequences of dropping self-gravity altogether, and integrating a system of test particles in the analytic field of the Hernquist halo plus the imposed bar. While the particle distribution gains some angular momentum, the density profile hardly changes when self-gravity is suppressed.

3.2. Cause of the density change

Resonances are very sharp in a fixed potential well with a steadily rotating disturbance. Once the few particles which start out close to these sharp resonances are scattered, or trapped, no more angular momentum can be gained by the halo. The fraction of particles affected by such artificially narrow resonances is too small to produce a significant change in the density profile in a system of test particles, as shown in Figure 2(c).

The very different behavior of all the models with self-gravity indicates that large density changes result from collective effects. The overall change in the mass profile seems to depend only on the bar strength, and not the numerical parameters (Figure 2). However, the rate of evolution does depend on two numerical parameters: the number of multipoles included in the calculation of halo self-gravity and the number of particles. I first consider what is happening in the large- N limit and then go on to discuss the dependence on numerical parameters.

3.2.1. Continuum limit

The bar scatters halo particles only at resonances in a steady potential. But the orbits of *all* particles, not just those in resonance, change when the gravitational potential well in which they move is altered. Not only does the wake develop, but the overall mass profile of the halo changes, because the scattered particles gain angular momentum and move to larger mean radii. As the potential well changes, more particles are able to become resonant and be scattered, causing further density changes. The process is gradual at first, but the changes accelerate as the density disturbance builds. Even though the process evidently runs away, it is not an instability because the

continuous supply of angular momentum from the bar is needed to drive the on-going re-arrangement of the density profile.

The runaway must end once the potential has changed sufficiently that no more particles are exposed to the principal resonance. The subsequent, more gradual changes seen in Figure 2 are probably caused by higher order resonances, which generally couple less strongly.

3.2.2. Numerical effects

The above mechanism may account for the behavior in the large- N limit, but we also observe that the runaway occurs earlier in grainier simulations. The number of particles at which the evolution slows to a rate that is independent of N is quite modest in some cases, and very large in others, but I have found convergence whenever I have tested for it.

The more rapid evolution at low N indicates that fluctuations due to the finite number of particles accelerate the density changes. Some particles which would not be resonant in a smooth potential can be scattered into resonance by fluctuations (an argument closely analogous to refilling of the loss-cone in AGN feeding and cometary dynamics). Thus the slow-build phase of the density change occurs more rapidly, and the runaway phase is reached earlier. Once the driven density changes exceed those arising from noise, the evolution will follow the same path as in a collisionless model.

Since the runaway is encouraged by fluctuations, it is reasonable that it could be delayed as N is increased, for a fixed number of multipoles. Further, one might naïvely expect adding more multipoles at fixed N would hasten the runaway, but the numerical evidence is that the low-order terms ($l = 1$ & 2) are of much greater importance than the intermediate order ($l = 3$ & 4). This is consistent with the picture (Earn & Sellwood 1995; Weinberg 1998) that much of the relaxation in N -body systems is driven by noise on global scales, probably through the excitation of neutrally-stable, low-order modes.

The importance of $l = 1$ is a surprise, however, since there is no obvious source of a dipole field. Since White (1983) reported that the dipole term caused a numerical artifact under some circumstances, I regarded this result with suspicion at first. However, tests showed that the rate of evolution with $l = 1$ active did not depend on such numerical parameters as grid resolution or particle number, and persisted even when the initial particle distribution was constructed to be perfectly bisymmetric with no net momentum. The rates of evolution both with and without the $l = 1$ terms were also reproducible with the SCF code. It is unlikely therefore that it is a numerical artifact. A dipole contribution could possibly arise from an instability related to that discovered by Taga & Iye (1998), although the physical situation is different; a deeper investigation is left for future work.

3.3. A shorter bar

WK01 find a short bar ($a = 0.5r_s$) can drive a large density decrease in an NFW halo in just 6 bar rotations in a simulation with 4M particles, which seems surprising given the trends in my Figure 2. I was unable to reproduce

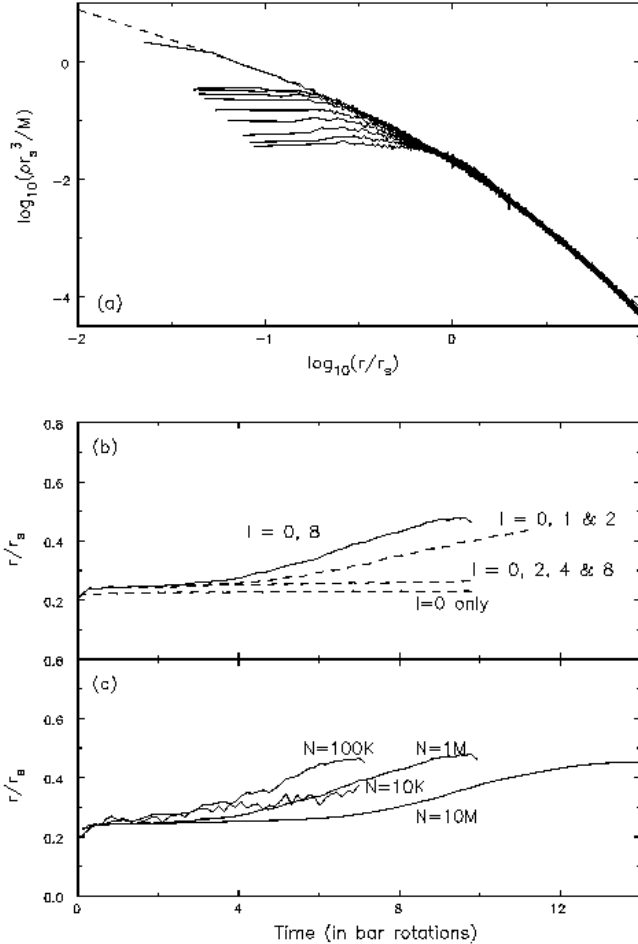


FIG. 3.— (a) The change in density profile of an NFW halo in an experiment that approximately reproduces the result reported in WK01. Curves are drawn at intervals of one initial bar rotations in this million particle experiment. (b) The radius containing 1% of the mass for several experiments with $N = 1M$. The solid curve shows the result from the simulation shown in (a), which includes terms $0 \leq l \leq 8$, and the dashed curves when the force terms were more restricted. (c) The dependence on the number of particles for these experiments with a short bar in an NFW halo. Terms $0 \leq l \leq 8$ are included in each case.

their result at first, but Weinberg (private communication) informed me that they employed more terms ($0 \leq l \leq 8$) in the field determination. When I include these additional terms in a simulation, I find the NFW halo, represented by 1M particles, does evolve quite rapidly as shown in Figure 3(a).

Figure 3(b) shows that the density change is substantially reduced when odd- l terms are omitted in the halo field calculation, and becomes minimal when the $l = 0$ term only is kept. These results are further support, of a similar kind, for the importance of the $l = 1$ terms. Generally, including terms $l > 2$ has a minor effect on the evolution rate, as can be seen in Figure 3(b).

As for the Hernquist halo, I find the rate of evolution generally slows for increasing N (Figure 3c), but the run with $N = 10K$ was so compromised by noise that it bucks this trend. The timescale increases substantially from $N = 1M$ to $N = 10M$, indicating that yet larger N is required for convergence when the halo is driven by a

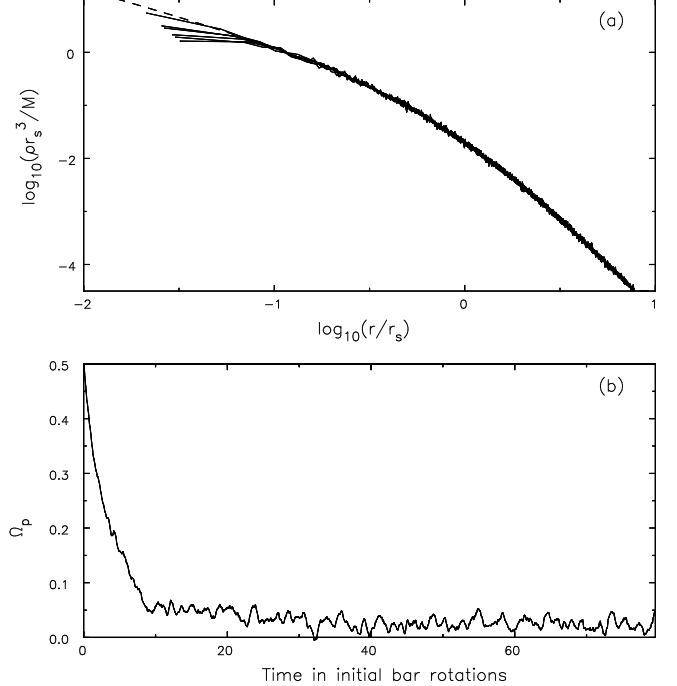


FIG. 4.— (a) The change in density profile of the Hernquist halo over the same time interval as shown in Figure 1 when angular momentum is conserved. Curves are drawn at intervals of 16 initial bar rotations. (b) The pattern speed of the bar which slows as it loses angular momentum.

steadily rotating short bar.

3.4. Angular momentum conservation

These simple tests are unphysical, because the bar is imposed and is driven at a fixed pattern speed. As already noted, the total angular momentum given to the halo exceeds the angular momentum of the bar ($L_{\text{bar}} = M_{\text{bar}}(a^2 + b^2)\Omega_p/9$ for an inhomogeneous Ferrers bar) by at least an order of magnitude. The pattern speed should therefore decrease rapidly as the bar torques up the halo.

Figure 4(b), which is for the same model and parameters as for Figure 1, shows that the bar slows rapidly when total angular momentum is conserved, *i.e.* the bar angular momentum is reduced as the halo gains. The angular momentum transferred in this case, shown by the dotted curve in Figure 1, causes a very minor decrease in the very inner part of the halo density (Figure 4a).

But rigid rod-like bars are unrealistic, in part because the effective moment-of-inertia of a responsive stellar bar is not simply related to its mass distribution. Fully self-consistent bar halo models, such as described in §4, offer much better tests.

3.5. Implications

The trend Figure 2(b) is that lower noise *delays* the density decrease, as WK01 also found in their SCF simulations. The better the simulation, the harder it becomes to drive a density change suggesting that the resonance(s) responsible for the large density change must already be present in experiments with quite low N .

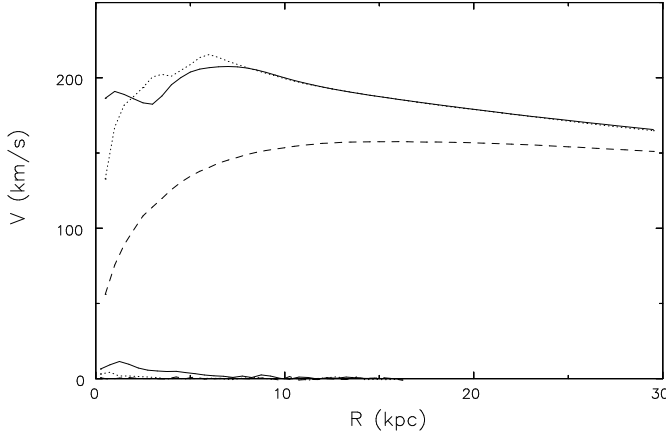


FIG. 5.— Rotation curves at three different times: the initial halo only (dashed), at the end of disk growth (dotted), and after the bar forms (solid). Also shown is the very small net rotation acquired by the halo by the end.

WK01 argue that 2-body scattering will prevent the correct angular momentum exchange with the bar, because an orbit suffers random impulses which destroy the important resonances. However, the empirical evidence from Figures 2 & 3 is that only the rate of evolution changes, while the overall angular momentum exchange is unaffected by the graininess. The reason their argument fails for these simulations is that scattering is due to large-scale potential variations, and is not of the direct 2-body kind. Any method to determine the gravitational field which smooths small-scale density variations suppresses direct 2-body scattering, causing orbits to approximate those in collisionless system, albeit in a global potential field which retains some stochastic jitter. It seems reasonable that approximately correct angular momentum exchange between particles and a bar could survive at low order resonances under these conditions. Their argument may remain valid for other N -body methods in which short-range interactions are more fully resolved.

These wholly artificial experiments, which showed such an encouraging reduction in the central density, are misleading for many reasons. Rigid bars driven at constant angular rates imply a huge external source of angular momentum and the density reduction is tiny when such a source is absent (Fig. 4). Also the choice of a constant pattern speed is inadvisable, because the true response when resonances are narrow requires more particles, as WK01 correctly point out.

It seems that the severe numerical difficulties presented by this totally artificial situation misled WK01 into arguing that simulations of extremely high quality are needed to get the physics right. In a sense, they are correct, since their artificial problem is so difficult, but needlessly so. Time-dependence of any aspect of the driving field, such as its strength or pattern speed, would broaden the resonances and expose a much larger fraction of particles to resonant interactions. Such experiments would be much easier, and quite modest simulations should quickly converge to the correct outcome.

A density runaway in the inner halo may yet be possible, although a very large amount of angular momentum must be delivered to the cusp to sustain it. El-Zant *et al.*

(2001) suggest that an orbiting satellite could have this effect on the inner density profile, as do Weinberg & Katz in their conference presentations. An orbiting satellite has much greater specific angular momentum than does a bar, and the halo density profile could be flattened significantly if coupling to the cusp can be arranged. El-Zant *et al.* estimate density changes in this situation without using N -body methods. Further experimentation is needed to determine how effectively the satellite can couple to the cusp.

4. FULLY SELF-CONSISTENT MODELS

Here I describe fully self-consistent models designed to investigate whether the halo density cusp could be erased through interactions with a responsive bar. These experiments required a new code, described in Appendix B, which is designed specifically to study isolated, near-equilibrium, disk+halo galaxy models. The method has the dynamic range to resolve collective modes in a realistic disk at the center of an extensive halo, while retaining the computational efficiency of a grid code.

4.1. Results

Creating fully-self consistent disk-halo equilibria is not straightforward and a number of increasingly sophisticated methods have been proposed (Hernquist 1993; Kuijken & Dubinski 1995; Debattista & Sellwood 2000). Since I wish to construct a model with a halo density profile resembling a compressed-NFW form, it is easier simply to grow the disk adiabatically within the halo.

I selected an isotropic Hernquist model for the halo (eq. 1), which is similar to NFW in the inner parts but the density declines more steeply at large radii. I grow a disk within the responsive halo by gradually adding particles on locally-determined circular orbits until the disk mass reaches the desired value, after which the model evolves freely. Provided the disk mass increases adiabatically, the precise procedure for creating the final model is immaterial (*e.g.* Binney & Tremaine 1987, §3.6), and guarantees an equilibrium starting point. I have run several calculations with different numerical parameters and different disk growth-rates to verify that the results are insensitive to the specific choices.

Figure 5 shows the rotation curve of one model, computed from the azimuthally averaged central attraction, at three different times: the initial halo, after disk growth and at the end of the calculation. The final disk is strongly self-gravitating; its mass is 1/20 of that of the halo while the exponential disk length scale length $R_D = r_s/8$. I have scaled the model, so as to resemble an NFW halo of concentration index ~ 10 : $R_D = 2$ kpc and $V_{\text{flat}} = 200$ km/s.

I have run several models with very similar physical parameters, but with the number of halo particles ranging from $2 \times 10^5 \leq N \leq 2 \times 10^7$; other numerical parameters are summarized in Table 1. Since I expanded the density on the spherical grid up to the $l_{\text{max}} = 4$ terms only, the halo particles feel only a rather fuzzy disk field when near the outer disk, but the full field of the bar is well represented. Tests with changing l_{max} showed that the bar-halo torque is almost entirely due to the large-scale $l = 2$ terms and the overall behavior is not all sensitive to increased expansion order.

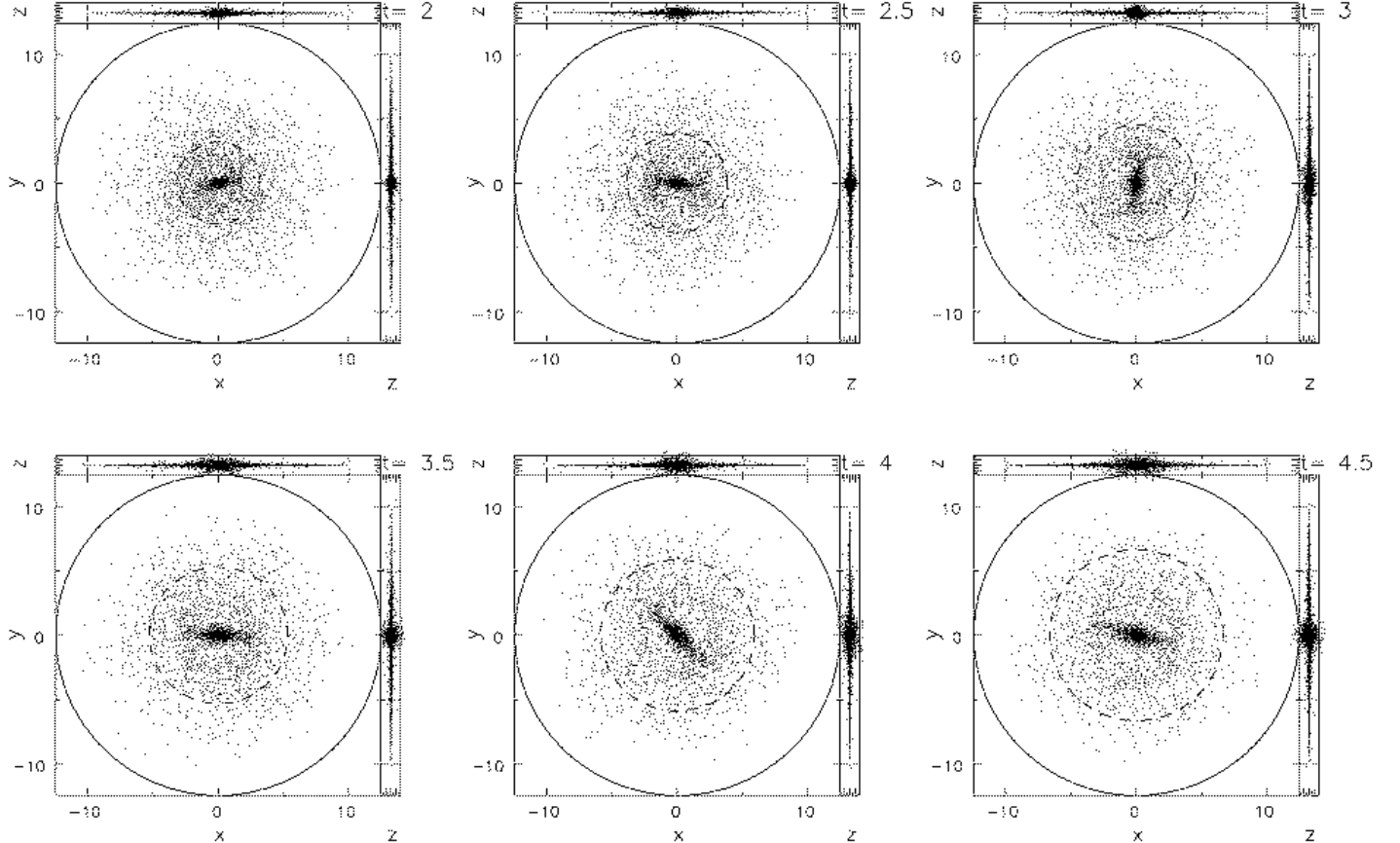


FIG. 6.— The later part of the evolution of the disk component. Only one particle in 200 is plotted. The dashed circles show the instantaneous radii of corotation. Times are in Gyr and distances in kpc.

TABLE 1

Numerical parameters used in the fully self-consistent simulations

	Cylindrical grid	Spherical grid
Grid size	$(N_R, N_\phi, N_z) = (81, 128, 125)$	$N_r = 500$
Angular compnts	$0 \leq m \leq 8$	$0 \leq l \leq 4$
Outer radius	12.4 kpc	320 kpc
z-spacing	12.5 pc	
Softening length	25 pc	
Largest N	1M	20M
Shortest time step	0.5 Myr	0.5 Myr

Results reported here are from the model with 20M halo particles and 1M disk particles; I do not find the evolution is significantly different for either one fourth or one twentieth this number. The model with just 200K halo particles and 10K disk particles did differ, however; it did not form a bar in the disk at all, presumably because noise heated the disk too much.

The mass of the exponential disk grows linearly over a period of 0.5 Gyr. As it nears its final value, the disk develops strong spirals, which are multi-armed at first, but are later dominated by $m = 3$ and some $m = 2$. A bar forms after about 1.2 Gyr; linear theory (Toomre 1981) would predict that a disk in a halo of this type is stable to

bar-modes, a prediction that has been verified in extremely high-quality simulations (Sellwood & Evans 2001). However, swing-amplified particle noise, which produces the spirals, leads to a bar through (non-linear) orbit trapping (e.g. Sellwood 1989) even for quite large particle numbers when, as here, the disk is highly responsive.

Figure 6 shows the later part of the evolution of the disk component. The half-length of the bar, a_B , was about 2 kpc, or only about 1/8 of the halo length scale, at first, but by 4.5 Gyr it had increased to about 3.5 kpc. The bar also slows down, as can be deduced from the corotation circle drawn by the dashed lines, to the extent that a_B is only about half the distance to corotation in the later stages of evolution. Such a slow bar is inconsistent with those observed (Aguerri *et al.* 2002).

Figure 7 shows the density profile of the halo at three times, together with the analytic density profile of the initial halo. The process of disk growth causes the halo to contract, of course, and the inner density profile steepens in the first 0.5 Gyr. The formation of the bar within the disk, which concentrates the disk mass, compresses the inner halo slightly more, giving the solid curve which stays constant until the end of the calculation at $t \simeq 5$ Gyr. Dynamical friction transfers angular momentum to the halo (Figure 7b), but the total amount is too small to reduce the halo density significantly. In fact, Figure 8 shows that the entire evolution is always towards a more compressed halo, caused by disk growth followed by on-going mass re-

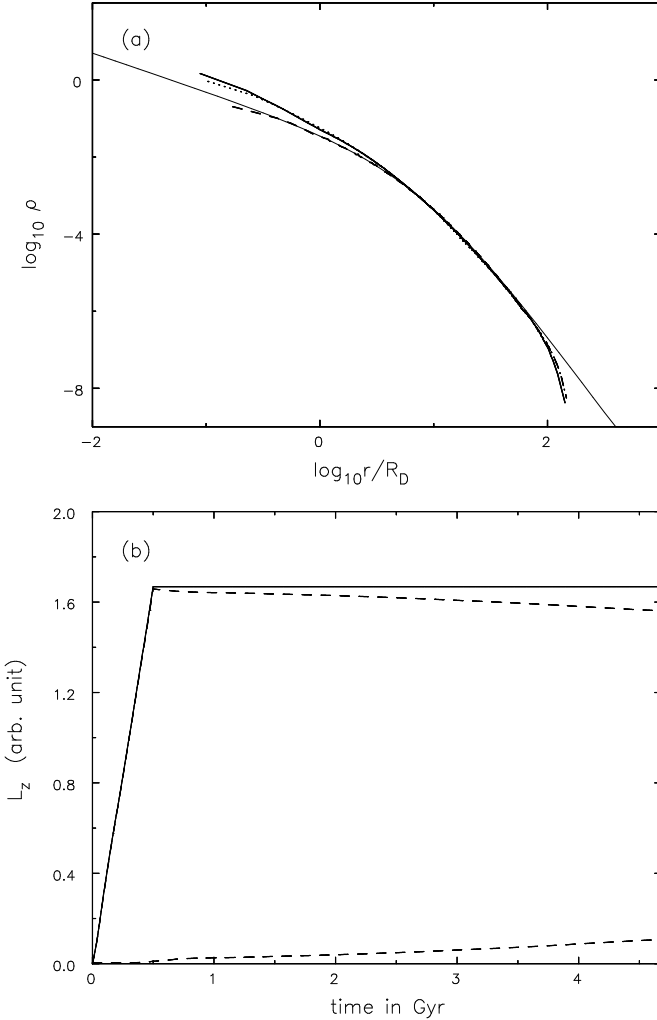


FIG. 7.— (a) The density profile of the halo in the simulation described in §4.1 at three different times. The smooth curve shows the theoretical Hernquist profile, while the dashed curve is measured from the particles at the start. The dotted curve shows the density profile after disk growth (0.5 Gyr) and the solid curve shows the profile at the end of the simulation (~ 5 Gyr). The break radius of the initial halo is $r_s = 8R_D$, and its truncation at $r = 160R_D$. (b) The total angular momentum of the model (solid curve) and the separate angular momenta of the disk and halo (dashed curves). The disk grows over the first 0.5 Gyr and then slowly loses angular momentum to the halo, which has none at first.

arrangement within the disk. Whatever density reduction of the inner halo that is being caused by bar scattering is being overwhelmed by the extra compression as the disk mass becomes more concentrated.

4.2. Discussion

Results from these models suggest that bars in fully-self-consistent disks with NFW-like halo models are too short ($0.125 \lesssim a_B/r_s \lesssim 0.25$) to erase the cusp by the method proposed by WK01. The bar length is determined by disk dynamics and is not, therefore, an adjustable parameter. More extensive halos with larger r_s or lower c might possibly allow longer bars to form, but I have so far failed to construct a realistic galaxy model (*i.e.* one having a quasi-flat rotation curve) which allows a large-enough bar to form in the disk that could conceivably erase the halo

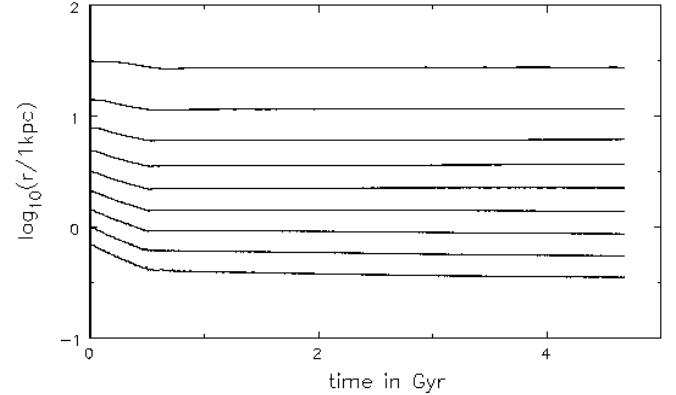


FIG. 8.— Radii enclosing various mass fractions as a function of time. Each line represents an increase of a factor 2 in enclosed mass, from 0.2% to 51.2% of the total NFW halo, which was truncated at 320 kpc.

cusp.

5. CONCLUSIONS

The results presented here indicate that the inconsistency between the cusped halos predicted from CDM models and the observed cores in galaxies cannot be removed by bar interactions. The suggestion by Weinberg & Katz (2001) that this might be possible was based on preliminary tests with large imposed bars with an unrealistic store of angular momentum.

Self-consistent bars do not contain enough angular momentum to change the halo density profile. Relatively short bars form in cuspy halos through disk “instabilities” on a scale controlled by the steeply rising rotation curve. The small bar exerts a correspondingly weak torque, and its small moment of inertia implies that little angular momentum is available to be transferred to the halo.¹

Additionally, as the bar forms, grows, and loses angular momentum, the mass distribution within the disk becomes more concentrated. The response of the halo is further compression which overwhelms any tendency for the inner halo density to decrease through its mild angular momentum gain.

I have also examined a number of numerical issues raised by WK01. The experiments they chose to illustrate the difficulties they describe were needlessly delicate because they contain extremely sharp resonances. More realistic tests in which the pattern speed declines as the bar loses angular momentum, have broader resonances and are therefore much easier. Nevertheless, I find that the density cusp can be flattened *more readily* in experiments with fewer particles in agreement with their findings with the SCF code. Even though the rate of evolution can be N -dependent, these simulations always converged to physically reasonable behavior that was independent of N . Conditions which require extremely high N are squarely in the needlessly difficult category. This does not, of course, imply that all N -body simulations can be trusted; those which are sloppily set up or fail to approximate the colli-

¹Larger bars might form in low-resolution simulations, because the steep rise in the inner rotation curve is inadequately resolved, but such simulations cannot address the issues raised here.

sionless limit should always be regarded with suspicion.

Martin Weinberg, who continues to disagree with some of my interpretations, has helped considerably with my understanding of the issues in this paper and has patiently borne an extensive e-mail correspondence and numerous discussions. Thanks are due to Victor Debattista for many helpful comments and for suggesting improvements to an early draft of the paper. Comments from Arthur Kosowsky and Eric Barnes were also helpful. This work was supported by NASA SARA grant NAG 5-10110 and by NSF grant AST-0098282.

REFERENCES

Aguerri, J. A. L., Debattista, V. P. & Corsini, E. M. 2002, MNRAS, to appear (astro-ph/0209377)

Binney, J. J. & Evans, N. W. 2001, MNRAS, **327**, L27

Binney, J., Gerhard, O. & Silk, J. 2001, MNRAS, **321**, 471

Binney, J. & Tremaine, S. 1987, *Galactic Dynamics* (Princeton: Princeton University Press)

Blais-Ouellette, S., Amram, P. & Carignan, C. 2001, AJ, **121**, 1952

Chandrasekhar, S. 1943, ApJ, **97**, 255

Courteau, S. 1997, AJ, **114**, 2402

Debattista, V. P. & Sellwood, J. A. 1998, ApJ, **493**, L5

Debattista, V. P. & Sellwood, J. A. 2000, ApJ, **543**, 704

de Blok, W. J. G., McGaugh, S. S. & Rubin, V. C. 2001, AJ, **122**, 2396

El-Zant, A., Shlosman, I. & Hoffman, Y. 2001, ApJ, **560**, 636

Ferrarese, L. & Merritt, D. 2000, ApJ, **539**, L9

Gebhardt, K., Bender, R., Bower, G., Dressler, A., Faber, S. M., Filippenko, A. V., Green, R., Grillmair, C., Ho, L. C., Kormendy, J., Lauer, T. R., Magorrian, J., Pinkney, J., Richstone, D. & Tremaine, S. 2000, ApJ, **539**, L13

Gnedin, O. Y. & Zhao, H.-S. 2002, MNRAS, bf 333, 299

Hernquist, L. 1990, ApJ, **356**, 359

Hernquist, L. 1993, ApJS, **86**, 389

Hernquist, L. & Barnes, J. E. 1990, ApJ, **349**, 562

Hernquist, L. & Ostriker, J. P. 1992, ApJ, **386**, 375

Hernquist, L. & Weinberg, M. D. 1992, ApJ, **400**, 80 (HW92)

Klypin, A., Gottlöber, S., Kravtsov, A. V. & Khokhlov, A. M. 1999, ApJ, **516**, 530

Kuijken, K. & Dubinski, J. 1995, MNRAS, **277**, 1341

Matthews, L. D. & Gallagher, J. S. 2002, ApJS, **141**, 429

McGlynn, T. A. 1984, ApJ, **281**, 13

Milosavljevic, M., Merritt, D., Rest, A. & van den Bosch, F. C. 2002, MNRAS, **331**, L51

Navarro, J. F., Eke, V. R. & Frenk, C. S. 1997, MNRAS, **283**, L72

Palunas, P. & Williams, T. B. 2000, AJ, **120**, 2884

Pfenniger, D. & Friedli, D. 1991, A&A, **252**, 75

Power, C., Navarro, J. F., Jenkins, A., Frenk, C. S., White, S. D. M., Springel, V., Stadel, J. & Quinn, T. 2002, astro-ph/0201544

Rubin, V. C., Burstein, D., Ford, W. K. & Thonnard, N. 1985, ApJ, **289**, 81

Sellwood, J. A. 1989, MNRAS, **238**, 115

Sellwood, J. A. 1997, in *Computational Astrophysics*, eds. D. A. Clarke & M. J. West (San Francisco: ASP Conference Series **123**), 215

Sellwood, J. A. & Athanassoula, E. 1986, MNRAS, **221**, 195

Sellwood, J. A. & Evans, N. W. 2001, ApJ, **546**, 176

Sellwood, J. A. & Merritt, D. 1994, ApJ, **425**, 530

Sellwood, J. A. & Valluri, M. 1997, MNRAS, **287**, 124

Swaters, R. A. *et al.* 2002, in preparation

Taga, M. & Iye, M. 1998, MNRAS, **299**, 111

Toomre, A. 1981, in *The Structure and Evolution of Normal Galaxies*, ed. S. M. Fall & D. Lynden-Bell (Cambridge: Cambridge University Press), p. 111

Tremaine, S. & Weinberg, M. D. 1984, MNRAS, **209**, 729

Valenzuela, O. & Klypin, A. 2002, astro-ph/0204028 (VK02)

van Albada, T. S. 1982, MNRAS, **201**, 939

van Albada, T. S. & van Gorkom, J. H. 1977, A&A, **54**, 121

Villumsen, J. V. 1982, MNRAS, **199**, 493

Weinberg, D. H., Hernquist, L. & Katz, N. 2002, ApJ, **571**, 15

Weinberg, M. D. 1985, MNRAS, **213**, 451

Weinberg, M. D. 1998, MNRAS, **297**, 101

Weinberg, M. D. 2001, in *Astrophysical Supercomputing Using Particles*, ed. J. Makino & P. Hut

Weinberg, M. D. & Katz, N. 2001, astro-ph/0110632 (WK01)

Weiner, B. J., Sellwood, J. A. & Williams, T. B. 2001, ApJ, **546**, 931

White, S. D. M. 1983, ApJ, **274**, 53

APPENDIX

A. SPHERICAL GRID

Several authors (van Albada & van Gorkom 1977; van Albada 1982; Villumsen 1982; White 1983; McGlynn 1984) have previously described N -body codes based on an expansion in surface harmonics. The potential at a field point (r, θ, ϕ) due to a number of point masses at $(r'_j, \theta'_j, \phi'_j)$ is the real part of

$$\Phi(\mathbf{r}) = -G \sum_{l=0}^{\infty} \sum_{m=0}^l (2 - \delta_{m0}) \frac{(l-m)!}{(l+m)!} \times P_l^m(\cos \theta) e^{im\phi} \left[\frac{A_{lm}}{r^{l+1}} + r^l B_{lm} \right]. \quad (A1)$$

where

$$A_{lm} \equiv \sum_{j,\text{int}} M_j P_l^m(\cos \theta'_j) e^{-im\phi'_j} r_j^l$$

$$B_{lm} \equiv \sum_{j,\text{ext}} M_j P_l^m(\cos \theta'_j) e^{-im\phi'_j} r_j^{l-(l+1)}. \quad (A2)$$

The summation for A_{lm} is over all particles for which $r'_j < r$, while all those with $r'_j > r$ are included in that for B_{lm} .

The two principal problems to be faced when using this formula for the forces in an N -body code are: (1) The errors in the calculated forces between a pair of particles at similar radii can be very large when the summations are truncated at a finite l_{\max} . Increasing l_{\max} reduces the radial extent of the region where the error is large, but also causes the errors over this shrinking region to worsen (just as Gibbs's phenomenon in Fourier series). (2) The forces acting between the pair of particles change discontinuously as they cross in radius – the problem known as “shell crossings.” Discontinuous changes in acceleration, when combined with a finite time-step size, cause particles to gain or lose energy for numerical reasons only. Villumsen (1982) and White (1983) introduce a softening parameter into the expressions for the potential, which smooths the forces but also creates a subtle artifact (White 1983). An alternative strategy (van Albada 1982), is to introduce a grid in all three coordinates. I have adopted the intermediate approach advocated by McGlynn (1984).

I introduce a 1-D radial mesh on which the coefficients A_{lm} and B_{lm} are tabulated, but retain the exact angular dependence, and therefore denote this method as PM+SH (standing for particle-mesh + surface harmonics). Concentric spheres at the set of radii $\{r_k\}$, $k = 0, n$ with $r_0 = 0$, divide the computation volume into onion-like shells. I improve slightly on McGlynn's method by interpolating between grid radii in the spirit of the cloud-in-cell procedure widely used in PM methods as follows: For a particle at radius r'_j , I locate the nearest r_k (which can be either interior or exterior to r'_j). I then give that particle the finite radial extent $\delta r'_j = \frac{1}{2}(r_{k+1} - r_{k-1})$, centred on r'_j . Thus fractions

$$w_{j,1} = \frac{1}{2} - \frac{r'_j - r_k}{\delta r'_j} \quad \text{and} \quad w_{j,2} = \frac{1}{2} + \frac{r'_j - r_k}{\delta r'_j} \quad (A3)$$

of the mass of particle j lie interior and exterior respectively to r_k . Exceptions to this rule occur at r_0 , where the entire mass of the particle is deemed to be exterior to the centre, and at r_n , where the entire mass of the particle is deemed to be interior to the outer edge.

The first step is to form the partial sum of the contributions from each particle fragment to the interior and exterior terms on each of its two neighbouring grid points, for each (l, m) :

$$\begin{aligned}\alpha_{lm}(k) &= \sum M_j w_{j,\nu} P_l^m(\cos \theta'_j) e^{-im\phi'_j} \frac{1}{r_k} \left(\frac{r'_j}{r_k}\right)^l \\ \beta_{lm}(k) &= \sum M_j w_{j,\nu} P_l^m(\cos \theta'_j) e^{-im\phi'_j} \frac{1}{r'_j} \left(\frac{r_k}{r'_j}\right)^l,\end{aligned}\quad (\text{A4})$$

where the summation for $\alpha_{lm}(k)$ [$\beta_{lm}(k)$] is over particle fragments, $\nu = 1, 2$, in the shell immediately interior [exterior] to r_k , but no further than r_{k-1} [r_{k+1}] *i.e.* every particle contributes to just four complex coefficients. (There are no contributions to $\alpha_{lm}(0)$ since no mass can be interior to $r = 0$.) Note that $\alpha_{lm}(k)$ and $\beta_{lm}(k)$ include the factors $r_k^{-(l+1)}$ and r_k^l in the particle's contribution to the coefficients $A_{lm}(k)$ and $B_{lm}(k)$ on sphere k . Since the ratio r_k/r'_j is close to unity, including these factors avoids multiplication (division) by large (small) numbers raised to high powers, as recommended by van Albada & van Gorkom (1977). (The exception for r_0 causes no difficulties since only the monopole term contributes at the center – the angular terms have no meaning.)

The next step is to sum over grid points so that a single coefficient on each grid point includes contributions from all the interior and exterior mass. This is a recursive sweep both inwards and outwards combining the previously obtained coefficients as follows:

$$\begin{aligned}A_{lm}(k) &= \alpha_{lm}(k) + A_{lm}(k-1) \left(\frac{r_{k-1}}{r_k}\right)^{l+1} \\ B_{lm}(k) &= \beta_{lm}(k) + B_{lm}(k+1) \left(\frac{r_k}{r_{k+1}}\right)^l.\end{aligned}\quad (\text{A5})$$

Note, this is the only step in the method for which the computation time depends on the number of grid radial grid points employed. Since there should be many fewer shells than particles, this single sweep in each direction represents a tiny overhead.

The potential is now defined on each sphere r_k and the acceleration vector can be computed as the negative gradient wrt the field coordinates. The expressions for the derivatives, though tedious, are straightforward. For the potential and acceleration components at general field points, where the particles are located, I interpolate linearly between shells for the radially dependent parts, but evaluate the angular part at the precise angular direction of the particle.

The source mass distribution is smoothed because the point mass particles are blurred both radially, by the grid and mass assignment scheme, and azimuthally, by the truncations at l_{\max} . The amount of radial smoothing is determined by the radial grid spacing. Forces acting on each particle change continuously as the particle crosses the grid

shells, although the gradient can be steep for large l_{\max} . Particles experience forces from others in the same shell (even themselves), but the relative contribution is small when N is large, because each particle has little mass, and the shells are thin, suggesting that the number of radial mesh points should vary with number of particles.

The radii of the grid points are completely arbitrary, but it is desirable to space them unevenly in order to obtain higher resolution near the center where the density is highest. I tried the strategy of spacing the shells so as to enclose precisely equal mass fractions, but find that the following rule leads to better results:

$$r_k = e^{\gamma k} - 1, \quad \text{with} \quad \gamma = \frac{\ln(r_n + 1)}{n} \quad (\text{A6})$$

where r_n is the desired radius of the outermost shell.

The overall computation time of the method scales almost perfectly as N times the number of azimuthal terms $(l_{\max} + 1)(l_{\max} + 2)/2$, because step (A5) is negligible. The code can be very efficiently adapted for parallel architectures; the best strategy is for each processor to work with a fraction of the particles. Once the partial sums (A4) have been formed on each, the only numbers which need to be communicated between processors are the rather small number of coefficients $\alpha_{lm}(k)$ and $\beta_{lm}(k)$.

B. HYBRID GRID N -BODY METHOD

Particle-mesh (grid) methods are the basis of the most efficient N -body codes (Sellwood 1997), and are therefore to be preferred for applications where they are viable. The traditional workhorse, the Cartesian grid, is barely adequate to resolve disk dynamics (Sellwood & Merritt 1994) and requires the halo to have a very limited extent and large quasi-uniform core (Debattista & Sellwood 2000). Adaptive grids (*e.g.* Klypin *et al.* 1999) are able to improve resolution wherever the particle density is high, but these locations are known and unchanging in our problem, and a fixed grid which concentrates resolution where it is needed will be more efficient.

No single fixed grid so far described has the ability resolve a thin disk, embedded within an extensive halo having a steep density gradient, however. Cylindrical polar grids (Pfenniger & Freidli 1991; Sellwood & Valluri 1997) offer better disk resolution than do Cartesian grids, but the number of grid planes becomes unmanageably large if the same grid must encompass an extensive halo, while uneven plane spacing is hopelessly inefficient. Spherical grids (Appendix A) on the other hand, are ideally suited to a near spherical mass distributions with a steep density gradient, but are unable to resolve the vertical structure of a disk component unless expanded to very high l_{\max} which is both expensive and undesirable.

I have therefore developed a hybrid PM scheme in which the self-gravity of the disk is computed on a high-resolution cylindrical polar grid while that of the halo is computed using the PM+SH method. As there is no restriction on the relative extents of the two grids, the initial disk can almost fill the cylindrical polar grid while the spherical grid has a radius many (here ~ 25) times larger.

Clearly, all particles must feel forces from all others at every step. Forces acting on disk particles within the smaller grid can be computed by interpolation on both

grids, but the field of the particles on the smaller grid cannot be extended outside that grid. I therefore define a second spherical grid, identical to the first, on which I calculate the forces from the disk to be added to the self-consistent halo field. Forces from the inner disk, bar and bulge are well represented by the spherical grid, even though the density distribution on the spherical grid is generally expanded to rather low l_{\max} . The strong vertical forces near the highly flattened outer disk are not well represented by the spherical grid, but that is the main purpose of the high-resolution small grid.

In order to avoid repeated discontinuous changes in forces for particles whose orbits take them into and out of the smaller grid volume, I label all halo particles as belonging to the larger grid, and use only accelerations determined for that grid wherever they may be. Thus, the halo particles feel only a rather fuzzy disk field when near the outer part of the disk; tests with increasing l_{\max} confirm that the overall dynamics is not significantly affected by this approximation. Disk particles which drift out of the smaller grid, are also relabelled as belonging to the larger grid for the rest of the calculation. If strong self-gravity of the outer disk is ever thought to be necessary as the disk spreads beyond the inner grid edge, it would be relatively inexpensive to increase the size of the inner grid.

The code allows particles to have individual masses, for their motion to be integrated using a range of time steps for greater efficiency, and has been implemented using the message-passing-interface (MPI) to enable its use on parallel machines with high efficiency.